34th Annual International Conference of the IEEE EMBS
San Diego, California USA, 28 August - 1 September, 2012

Unsupervised Tumour Segmentation in PET based on Local and Global Intensity Fitting Active Surface and Alpha Matting

Ziming Zeng[1], Tony Shepherd[2] and Reyer Zwiggelaar[3]

Abstract— **This paper proposes an unsupervised tumour segmentation scheme for PET data. The method computes the volume of interests (VOIs) with subpixel precision by considering the limited resolution and partial volume effect. Firstly, it uses local and global intensity active surface modelling to segment VOIs, then an alpha matting method is used to eliminate false negative classification and refine the segmentation results. We have validated our method on real PET images of head-and-neck cancer patients as well as images of a custom designed PET phantom. Experiments show that our method can generate more accurate segmentation results compared with alternative approaches.**

I. INTRODUCTION

Positron emission tomography (PET), which is one of the most advanced medical imaging technologies on the molecular level of human functional imaging, can provide an important basis for the early diagnosis and treatment of brain, cardiovascular, nervous system and malignant disease. Segmentation of PET VOIs has become important for modern treatment planning and is commonly performed manually or by thresholding standardised uptake values (SUVs) [1]. Manual segmentation uses a combination of PET and reference images from CT or MRI, but observer-variability is high [2]. Thresholding lies at the core of most fully- or semi-automatic PET segmentation [3], but overlooks heterogeneity in the case of tumours and performs poorly for low spatial resolution and signal-to-noise properties typical in PET oncology. More advanced methods include the Poisson Gradient Vector Flow (PGVF) of Hsu et al. [4] for edge-based segmentation, the Markov Random Field Expectation Maximisation (MRF EM) labelling technique of Gribben et al. [5]. These methods only consider intensity and spatial characteristics of PET images, but ignore the information of the whole volume. Also, these methods are hindered by poor spatial resolution and partial volume effects (PVE). To address these, we propose a new VOI segmentation method which employs local and global intensity active surface modelling and alpha matting. Experimental results show that this approach is robust with respect to noise and density inhomogeneity in PET data, and can achieve accurate segmentation results.

[1]Ziming Zeng is with the Faculty of Information and Control Engineering, Shenyang Jianzhu University, Shenyang, China, and with the Department of Computer Science, Aberystwyth University, UK zzz09@aber.ac.uk

[2]Tony Shepherd is with the Turku PET Center and Department of Oncology and Radiotherapy, Turku University Hospital, Finland. tony.shepherd@tyks.fi

[3]Reyer Zwiggelaar is with the Department of Computer Science, Aberystwyth University, UK rrz@aber.ac.uk

II. IMAGE SEGMENTATION METHOD

As a pre-processing step, significantly noisy images are discarded before 3D volumes are generated. Then image intensity is normalized in the 0 – 255 range. Subsequently, we use a 3×3×3 median filter to reduce noise. The remaining segmentation algorithm is hierarchical, consisting of three steps. In the first step, we detect whether tumours exist, and a threshold is auto-estimated which is used for the local and global intensity active surface to segment the tumours. In the second step, a alpha matting approach is used to find non-detected regions. In the third step, a more robust trimap which contains a definite foreground, a definite background and an unknown region is automatically generated and an alpha matting technique is used to refine the segmentation results. The process is shown in Fig. 1.

A. Tumour Detection and Voulme Segmentation

In this first step, the maximum grey level value for each slice is extracted, and all the values are normalized to 0 – 1. Then we calculate the standard deviation of all the maximum values of the slices which contain tissues. If the results is above a threshold τ, we assume that this volume contains tumour. In the segmentation step, we use intensity based active surface modelling [6], which considers both local and global intensity aspects. As in [6], the energy function is formally defined as:

$$\mathcal{F}(\phi, c_1, c_2, f_1, f_2) = \mathcal{E}^{LGIF}(\phi, c_1, c_2, f_1, f_2) + \mu\mathcal{P}(\phi) + \upsilon\mathcal{L}(\phi) \quad (1)$$

$$\mathcal{E}^{LGIF}(\phi, c_1, c_2, f_1, f_2) = (1-\omega)\mathcal{E}^{LIF}(\phi, f_1, f_2) + \omega\mathcal{E}^{GIF}(\phi, c_1, c_2) \quad (2)$$

where ϕ denotes the tumour contour, ω is a positive constant. $\mathcal{P}(\phi) = \int (1/2)(\mid \nabla\phi(x) \mid -1)^2 dx$ is the level set regularization term, $\mathcal{L}(\phi) = \int (\mid \nabla H(\phi(x)) \mid) dx$ is the smoothing term. $\mathcal{E}^{LIF}$ is the local energy function and $\mathcal{E}^{GIF}$ is the global energy function, which are defined as

$$\mathcal{E}^{LIF}(\phi, f_1, f_2) = \sum_{i=1}^{2} \lambda_i \int [\int K_\sigma(x-y) \mid f_i(x) - I(y) \mid^2 M_i(\phi(y)) dy] dx \quad (3)$$

$$\mathcal{E}^{GIF}(\phi, c_1, c_2) = \sum_{i=1}^{2} \int [\int \mid I(x) - c_i \mid^2 M_i(\phi(x))] dx \quad (4)$$

where $K_\sigma(u)$ is a 3D Gaussian kernel function. $K_\sigma(x-y)$ is a weight on point y with regard to the center point x. The local fitting energy $\mathcal{E}^{LIF}$ is determined by the value of σ. $M_1(\phi) = H(\phi), M_2(\phi) = 1 - H(\phi)$. The Heaviside function H is usually approximated by a smooth function $H_\epsilon(x) = (1/2)[1+(2/\pi)arctan\,(x/\xi)]$. As the grey level of tumours can

978-1-4577-1787-1/12/$26.00 ©2012 IEEE

vary between volumes, Zeng et al. [7] changed this function to

$$H_\epsilon(x) = \frac{1}{2}\left[1 + \frac{2}{\pi} arctan\left(\frac{x-T}{\xi}\right)\right] \quad (5)$$

where T $(0 \leq T \leq 1)$ denotes a tumour grey level threshold. It is the average of maximum grey level value of some slices. Specifically, we obtain the maximum value in each slice (see Fig. 1, step 1) and use the maximum grey level value across the slices as a starting point. To the left and the right we propagate across the selected slices until the difference between the slice maximum and the maximum in subsequent slices is above a threshold φ. This range indicates the slices to be used.

According to the derivation by Wang et al. [6], the optimal functions $f_1(x)$, $f_2(x)$ and constants c_1, c_2 that minimize $\mathcal{F}(\phi, c_1, c_2, f_1, f_2)$ are:

$$f_i(x) = \frac{K_\sigma(x) * [M_i(\phi(x))I(x)]}{K_\sigma(x) * M_i(\phi(x))}.i = 1, 2 \quad (6)$$

$$c_i(x) = \frac{\int I(x)M_i(\phi(x))dx}{\int M_i(\phi(x))dx}.i = 1, 2 \quad (7)$$

The optimal fitting functions $f_1(x)$, $f_2(x)$ and constants c_1, c_2 that minimize the energy function ϕ can be written as:

$$\frac{\partial \phi}{\partial t} = \delta(\phi)\left[\upsilon div\left(\frac{\nabla\phi}{\mid \nabla\phi \mid}\right) - (F_1 + F_2)\right] + \mu\left(\nabla^2\phi - div\left(\frac{\nabla\phi}{\mid \nabla\phi \mid}\right)\right) \quad (8)$$

where δ is the derivative of H_ϵ. The local intensity force F_1 and the global intensity force F_2 are defined as:

$$F_1 = (1-\omega)[\int K_\sigma(y-x) \mid I(x) - f_1(y) \mid^2 dy - \int K_\sigma(y-x) \mid I(x) - f_2(y) \mid^2 dy] \quad (9)$$

$$F_2 = \omega[(I(x) - c_1)^2 - (I(x) - c_2)^2] \quad (10)$$

In [6], the energy function of the local and global model in Eq. 8 is not convex and the evolution by using the gradient descent can easily be trapped into a local minimum. In this work, we apply the global convex segmentation model [8] to make the energy fitting convex. Specifically, the simplified flow represents the gradient descent for minimizing the energy: $E(\phi) =\mid \nabla\phi \mid_1 + \langle \phi \cdot r \rangle$, where $r = F_1 + F_2$. Yang et al. [9] restricted the solution to lie in a finite interval in order to transform the constrained optimization problem to an unconstrained one. In this work, we constrain ϕ to $0 \leq \phi \leq 1$, which can guarantee a unique global minimal. The global convex model can be written as $min_{0\leq\phi\leq1}E(\phi) = min_{0\leq\phi\leq1}(\mid \nabla\phi \mid_1 + \langle \phi \cdot r \rangle)$. In [9], the minimization problem has been written as

$$min_{0\leq\phi\leq1}E(\phi) = min_{0\leq\phi\leq1}(\int g \mid \nabla\phi \mid + \langle \phi \cdot r \rangle) \quad (11)$$

where $g(\Theta) = 1/(1 + \beta \mid \Theta \mid^2)$, β is a constant value. Then the Split Bregman method is used to minimize the energy function [9]. When the optimal ϕ is found, we can find the segmented region $\Omega^k = \left\{x : \phi^k(x) > 0.5\right\}$.

By using the above segmentation method, the VOIs in the PET volume can be segmented and a reliability metric is used to remove false positive VOIs. Specifically, the 6-connected neighborhood voxels are labeled in the results, and if the tumor only exist in one or two slices, then corresponding 3D labelling will be removed from the results. The segmentation results have limited accuracy and some abnormal tissues may not be detected because of the limited image resolution.

B. Non-detected Region Segmentation

In the second step, we propose a false negative searching criterion to identify the non-detected regions. The method searches for the non-detected tumours from two directions across the slices (from top to bottom and from bottom to top). Firstly, the first slice containing tumour pixels is detected in a search sequence from the top. Then morphology and alpha matting [10] are used to generate a soft segmentation result. The pixel values of the segmentation result are between 0 and 1, and we use the pixels which are above ψ as a mask region to extract the corresponding pixels in the current slice and the next slice. If the difference of the extracted grey level value in the same position of the two slices is below a threshold β, this pixel will be superimposed on the segmentation results in the next slice. In this way, the segmentation results can be propagated to the other slices from the top to bottom direction, and some non-detected regions can be found. Then the same process is also imposed for the bottom to top direction. Finally, we use half the maximum grey level value to generate two binary segmentations as indicated in step 2 in Fig. 1.

In step 2, before using the alpha matting method, a trimap is required which includes three regions: definite foreground, definite background and unknown region. Specifically, for each slice, we use the binary segmentation result as the foreground. Subsequently, morphology is used to erode and dilate the segmentation result with a circular structuring element. The unknown region is the difference between the erosion and dilation areas, and the background is the remaining region. Each single slice can be modeled as $I_i = \alpha F_i + (1-\alpha)B_i$, where I is the observed image, F and B are foreground and background, and alpha is the transparency parameter between 0–1. This model can be rewritten as $\alpha_i = aI_i + b$, where $a = 1/(F-B)$, $b = -B/(F-B)$. To solve the alpha matting problem, Levin et al. [10] converted the problem to finding α, a and b to minimize the cost function

$$J(\alpha, a, b) = \sum_{j\in I}\left(\sum_{i\in w_j}(\alpha_i - a_jI_i - b_j)^2 + \varepsilon a_j^2\right) \quad (12)$$

where w_j is a small window around pixel j. For $J(\alpha) = min_{a,b}J(\alpha, a, b)$, we have $J(\alpha) = \alpha^T L\alpha$, where

$$L_{i,j} = \sum_{k\mid(i,j)\in w_k}\left(\delta_{i,j} - \frac{1}{\mid w_k \mid}\left(1 + \frac{(I_i-\mu_k)(I_j-\mu_k)}{\frac{\varepsilon}{\mid w_k \mid} + \sigma_k^2}\right)\right) \quad (13)$$

In this Laplacian function, $\delta_{i,j}$ is the Kronecker delta, μ_k and σ^2 are the mean and variance of the intensities in the window w_k around k which is usually 3×3, and $\mid w_k \mid$ is the number of pixels in this window. The details of the energy minimization process can be found in [10].

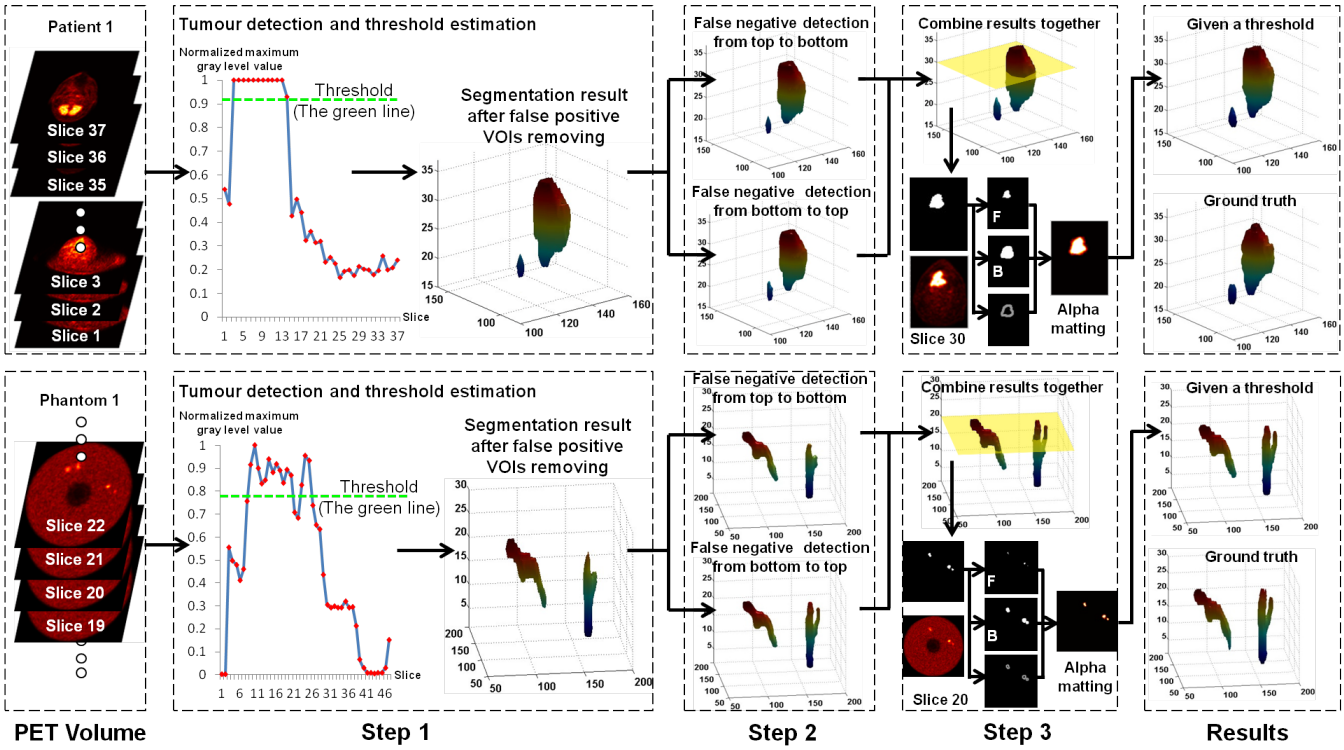

Fig. 1. Segmentation results of our proposed approach. The top and the bottom groups show the processing on Patient 1 and Phantom 1 volume, respectively.

C. *Refining Segmentation Results*

In the third step, we use the || *or* operator to combine the previous two volumes into one binary result, and some non-detected regions can be effectively detected. However, the result is not accurate enough due to partial volume effects. For some slices containing tumours, we can easily erode and dilate the binary results to give a robust trimap, and the alpha matting method can be used again to refine the previous segmentation results, as is shown in step 3 in Fig. 1. But for some regions which are very small, erosion will remove all pixels. In our work, to address this problem, we label the segmented regions in each slice, if the number of pixels in a labelled region is smaller than 9, the labelled region will be directly used as the foreground without erosion.

III. EXPERIMENTS

To indicate the accuracy of the proposed method, we use 2 PET images of head-and-neck cancer patients and 2 images of a custom-built tumour phantom [11], [12]. All images were acquired using a hybrid PET/CT scanner (GE Discovery) and the metabolic tracer [^{18}F]FDG. Ground-truth VOIs needed for segmentation evaluation were obtained independently for both phantom and patient images. Phantom ground truth was determined by thresholding the simultaneous CT images at the density of glass. In the case of patient tumours, ground-truth segmentations were estimated using manual delineation by three separate expert physicians based at the imaging site. Each expert delineated each patient tumours twice, viewing both PET and CT images together. From the resulting 6 expert delineations we select one as the ground truth.

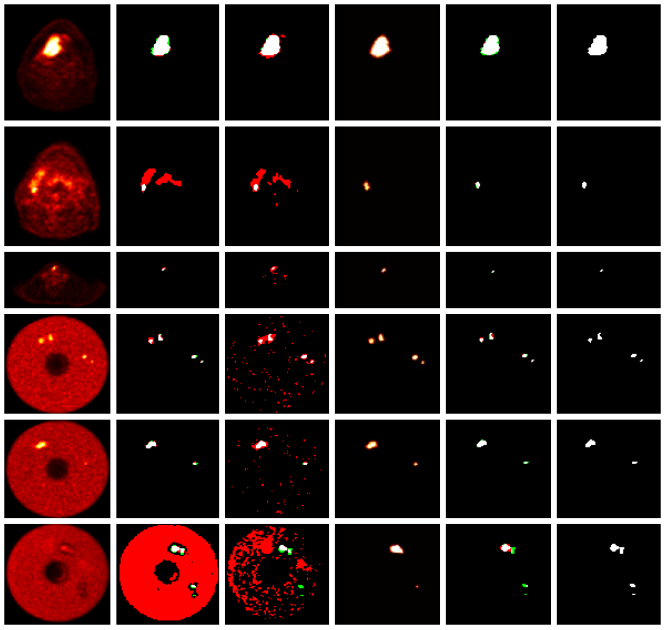

Fig. 2. Segmentation of VOIs (red: false positive, green: false negative, white: true positive, black: true negative). From left to right, PET data; patient data (slice 28, slice 21 for patient 1, and slice 9 for patient 2), phantom data (slice 22, slice 26 for phantom 1, and slice 21 for phantom 2), PGVF [4]; MAP-MRF EM [5]; soft segmentation results by using our method; binary results (half of the maximum grey level value of our results); ground truth.

The detailed segmentation process for the example of a patient tumour and a phantom tumour are shown in Fig. 1. In the first step, the significant noise images are discarded, then the maximum grey level values for each slice is normalize between 0 – 1. For the slices with tissues, the standard deviation is calculated as 0.351 and 0.173 on Patient 1 and Phantom 1 volume, respectively. In our method, the tumour determination threshold τ is defined as 0.05. Subsequently, the selected slices (patient 1: from 2 to 15, phantom 1: from 7 to 30) are identified using the proposed criteria ($\varphi = 0.12$), then the threshold T in Eq. 5 is automatically estimated as 0.916 and 0.783, respectively. In this work, $\omega = 0.1$ in Eq. 2, the 3D Gaussian kernel σ is 3, $\lambda_i = 10$ in Eq. 3, $\xi = 0.1$ in Eq. 5. The improved active surface modelling result is used to segment the image and false positive regions are automatically removed. In the second step, a search criteria for non-detected region is used. A circular structuring element (3 pixels radius for patient 1, 7 pixels radius for phantom 1) is used for dilation: the pixels radius is associated with the image resolution in our work. In this work, the parameter $\psi = 0.85$ and $\beta = 17$. From the results in Fig. 1, we can see some none-detected regions can be identified. In the third step, the alpha matting algorithm is used to refine the segmentation. The radius for dilation and erosion, which are 4 and 2 respectively are used for all the images. To compare against the ground truth which is a binary image, we threshold the soft segmentation generated by matting at half of the maximum grey level value for each slice, which leads to the final binary segmentation of VOIs.

We compare our method with alternative approaches on real and phantom PET data. In Fig. 2, for the real PET data, comparing with the ground truth, the results of PGVF and MAP-MRF EM methods have more false positives (in red) than our results, especially on the slice 21 for patient 1. The problem is partly explained by the low spatial resolution of the images and partial volume effects but could also be due to these slice-wise methods ignoring volumetric grey level information. For the phantom data, the PGVF method fails to segment the abnormal region, because the density of the abnormal region is similar to the surrounding tissue. It also does not perform well by using MAP-MRF EM method on images with significant noise. In contrast, the developed method performs well with these images and provides accurate segmentation results.

We evaluate segmentation accuracy in terms of overlap with ground-truth by using the Dice similarity coefficient (DSC). We compare the DSC of our method and alternative approaches [4], [5]. Tab. I shows the mean DSC for real and phantom PET as well as the overall mean. Our results show improvements compared to alternative approaches.

TABLE I

DICE INDEX FOR TUMOUR SEGMENTATION ON PET DATA

Algorithm	PGVF [4]	MAP-MRF EM [5]	Our method
Patient images	0.570	0.402	0.734
Phantom images	0.423	0.383	0.632
All images	0.497	0.393	0.683
Standard deviations	0.252	0.228	0.168

IV. DISCUSSION AND CONCLUSIONS

In this paper, we introduce a new scheme for PET image segmentation based on an improved local and global intensity based active surface and alpha matting method. Firstly, the segmentation method uses the local and global information to segment the volume data, which can largely eliminate segmentation errors. Secondly, a searching criterion for non-detected region is used, which can effectively find false negatives. Thirdly, the alpha matting technique is introduced to deal with the partial volume effects, which can lead to subpixel precision for the results. Finally, compared with alternative approaches, our method is more robust on PET imaging segmentation. In the future, we will use the average of manually segmentation results as the ground truth to evaluate our method. Also, this method will be evaluated on a larger clinical PET database and will be applied on the other medical imaging modalities.

REFERENCES

[1] Y.Nakamoto, K.R.Zasadny, H.Minn, and R.L.Wahl, Reproducibility of common semi-quantutative parameters for evaluating lung cancer glucose metabolism with positron emission tomography using 2-deoxy-2-[18F]Fluoro-D-Glucose, Molecular Imaging Biology, vol. 4, 2002, pp. 171-178.

[2] S.L.Breen, J.Publicover, S.DeSilva, G.Pond, K.Brock, B.OSullivan, B.Cummings, L.Dawson, A.Keller, J.Kim, J.Ringash, E.Yu, A.Hendler, and J.Waldron, Intraobserver and interobserver variability in GTV delineation on FDG-PET-CT images of head and neck cancers, International Journal of Radiation Oncology Biology Physics, vol. 68, 2007, pp. 763-770.

[3] Y.E.Erdi, O.Mawlawi, S.M.Larson, M.Imbriaco, H.Yeung, R.Finn, and J.L.Humm, Segmentation of lung lesion volume by adaptive positrone mission tomography image thresholding, Cancer, vol. 80, 1997, pp. 2505-2509.

[4] C.Hsu, C.Liu, and C.Chen, Automatic segmentation of liver PET images, Computerized Medical Imaging and Graphics, vol. 32, 2008, pp. 601-610.

[5] H.Gribben, P.Miller, H.Wang, K.Carson, A.Hounsell, and A.Zatari, Automated MAP-MRF EM labelling for volume determination in PET, in 2008 Proc. ISBI Conf., pp. 1-4.

[6] L.Wang, C.M.Li, Q.S.Sun, D.S.Xia, and C.Y.Kao, Brain MR image segmentation using local and global intensity fitting active contours/surfaces, Lecture Notes in Computer Science, vol. 5241, 2008, pp. 384-392.

[7] Z.Zeng, T.Shepherd, and R.Zwiggelaar, Hierarchical Modelling for Unsupervised Tumour Segmentation in PET, in 2012 Proc. BHI Conf., pp. 439-443.

[8] T.F.Chan, S.Esedoglu, and M.Nikolova, Algorithms for finding global minimizers of denoising and segmentation models, SIAM Journal on Applied Mathematics, vol. 66, 2006, pp. 1632-1648.

[9] Y.Yang, C.Li, C.Kao, and S.Osher, Split Bregman method for minimization of region-scalable fitting energy for image segmentation, Lecture Notes in Computer Science, vol. 6454, 2010, pp. 117-128.

[10] A.Levin, D.Lischinski, and Y.Weiss, A closed form solution to natural image matting, Pattern Analysis and Machine Intelligence, vol. 30(2), 2008, pp. 228-242.

[11] T.Shepherd, M.Teräs, and H.Sipilä, New Physical Tumour Phantom and Data Analysis Technique Exploiting Hybrid Imaging and Partial Volume Effects for Segmentation Evaluation in Radiation Oncology, European Journal of Nuclear Medicine and Molecular Imaging, vol. 37, 2011, pp. S221.

[12] T.Shepherd, M.Teräs, R.Beichel, R.Boellaard, M.Bruynooghe, V.Dicken, M.Gooding, P.Julyan, J.Lee, S.Lefèvre, V.Naranjo, U.Nestle, X.Wu, H.Zaidi, Z.Zeng and H.Minn, Comparative Study with New Accuracy Metrics for Target Volume Contouring in PET Image Guided Radiation Therapy. IEEE Transactions on Medical Imaging, in press, June 2012.